

RESEARCH ARTICLE

10.1002/2016MS000725

# The impact of the diurnal cycle on the propagation of Madden-Julian Oscillation convection across the Maritime Continent

Samson M. Hagos<sup>1</sup>, Chidong Zhang<sup>2</sup>, Zhe Feng<sup>1</sup>, Casey D. Burleyson<sup>1</sup>, Charlotte De Mott<sup>3</sup>, Brandon Kerns<sup>2</sup>, James J. Benedict<sup>2</sup>, and Matus N. Martini<sup>4</sup>

<sup>1</sup>Pacific Northwest National Laboratory, Richland, Washington, USA, <sup>2</sup>University of Miami, Miami, Florida, USA, <sup>3</sup>Colorado State University, Fort Collins, Colorado, USA, <sup>4</sup>Naval Research Laboratory, Monterey, California, USA

**Key Points:**

- The diurnal cycle disrupts MJO propagation across the Maritime Continent
- It enhances downwelling radiation and precipitation over the MC islands
- It however has a net cooling effect on the MC land surfaces

**Correspondence to:**

S. Hagos, samson.hagos@pnnl.gov

**Citation:**

Hagos, S. M., C. Zhang, Z. Feng, C. D. Burleyson, C. De Mott, B. Kerns, J. J. Benedict, and M. N. Martini (2016), The impact of the diurnal cycle on the propagation of Madden-Julian Oscillation convection across the Maritime Continent, *J. Adv. Model. Earth Syst.*, 8, 1552–1564, doi:10.1002/2016MS000725.

Received 26 MAY 2016

Accepted 15 SEP 2016

Accepted article online 19 SEP 2016

Published online 8 OCT 2016

**Abstract** Influences of the diurnal cycle on the propagation of the Madden-Julian Oscillation (MJO) convection across the Maritime Continent (MC) are examined using cloud-permitting regional model simulations and observations. A pair of ensembles of control (CONTROL) and no-diurnal cycle (NODC) simulations of the November 2011 MJO episode are performed. In the CONTROL simulations, the MJO signal is weakened as it propagates across the MC, with much of the convection stalling over the large islands of Sumatra and Borneo. In the NODC simulations, where the incoming shortwave radiation at the top of the atmosphere is maintained at its daily mean value, the MJO convection signal propagating across the MC is enhanced. Examination of the surface energy fluxes in the simulations indicates that the surface downwelling shortwave radiation is larger in the presence of the diurnal cycle (CONTROL simulations) primarily because clouds preferentially form in the afternoon and are smaller during day time in comparison to nighttime. Furthermore, the diurnal covariability of surface wind speed and skin temperature results in a larger sensible heat flux and a cooler land surface in the CONTROL runs compared to NODC runs. An analysis of observations indicates that ahead of and behind the MJO active phase, the diurnal cycle of cloudiness enhances downwelling shortwave radiation and hence convection over the MC islands. This enhanced stationary convection competes with and disrupts the convective signal of MJO events that propagate over the waters surrounding the islands.

## 1. Introduction

The Indo-Pacific Maritime Continent (MC) is a unique geographical region with many islands and semienclosed seas straddling the equator. It has long been recognized as a barrier for the eastward propagation of the Madden-Julian Oscillation (MJO) [Rui and Wang, 1990; Salby and Hendon, 1994]. Upon arriving at the MC, MJO events behave in a rather erratic and unpredictable manner. Some slowly propagate eastward, some stall and/or terminate, and others end up with a center of convection split into branches over the larger islands [Rui and Wang, 1990; Salby and Hendon, 1994; Zhang and Hendon, 1997; Hsu et al., 2005]. This disruption of MJO propagation by the MC is exaggerated in many numerical models [Kim et al., 2009; Jiang et al., 2015]. The MJO forecast skill is often low over the MC because of this so-called “MJO prediction barrier” of the MC [Seo et al., 2009; Vitart and Molteni, 2010]. Recent work by Neena et al. [2014] suggests that the MC is not an intrinsic predictability barrier and can be overcome with improved models. It is unclear what processes control this erratic MJO behavior over the MC and the associated modeling and prediction difficulties. One possible reason for the prediction barrier is the interaction between the MJO and the diurnal cycle of convection over the MC.

Several studies have documented the influence of the MJO on the diurnal cycle of convection over the MC [e.g., Rauniyar and Walsh, 2011; Peatman et al., 2014; Birch et al., 2016]. In a conceptual framework of the MJO where the convection follows the availability of moist static energy (MSE), several studies have shown that when the main MJO convective envelope is over the Indian Ocean, rainfall and its diurnal cycle over the MC islands reach their maxima with strong land-sea breeze circulations due to high MSE supply by solar insolation occurring in a relatively unstable environment. Subsequently, cloud cover increases and surface insolation decreases as the convective envelope of the MJO arrives at the MC, which in turn weakens the rainfall over the islands [Rauniyar and Walsh, 2011]. This occurs even though the large-scale environment remains favorable for convection at this time. While these studies show a clear influence of the MJO on the

© 2016. The Authors.

This is an open access article under the terms of the Creative Commons Attribution-NonCommercial-NoDerivs License, which permits use and distribution in any medium, provided the original work is properly cited, the use is non-commercial and no modifications or adaptations are made.

**Table 1.** Configuration Common to All Simulations

Parameter or Initial Condition	Configuration
Grid spacing	4 km
Cumulus parameterization	None
Longwave radiation parameterization	The Rapid Radiative Transfer Model [Mlawer <i>et al.</i> , 1997]
Shortwave radiation parameterization	The Rapid Radiative Transfer Model [Morcrette <i>et al.</i> , 2008]
Microphysics parameterization	Thompson [Thompson <i>et al.</i> , 2008]
Boundary layer parameterization	Yonsei State University scheme [Hong and Dudhia, 2006]

diurnal variability of convection over the MC, the feedback of the latter on to the progression of the MJO convection is potentially an important mechanism that may provide clues as to why some MJO

convection events stall or weaken while others remain strong when they cross the MC. Such a mechanism remains largely unexplored. Using an idealized analytical model, Majda and Yang [2016] show that planetary-scale diurnal variability of diabatic heating can have an upscale effect on intraseasonal variability via the eddy flux divergence of potential temperature. Specifically the heating from the upscaled planetary-scale diurnal temperature fluctuations can cancel temperature anomalies associated with the MJO diurnal cycle. Thus, they suggest this mechanism might explain the weakening of MJO signals over the MC. Our study examines the influence of the diurnal cycle on the propagation of MJO convection across the MC using cloud-permitting regional model simulations and observations.

## 2. Simulations and Observations

### 2.1. Simulation Design

The modeling component of this study focuses on the November 2011 MJO episode that propagated over the MC. This MJO event was extensively documented by using observations from the Atmospheric Radiation Measurement (ARM) Madden-Julian Oscillation (MJO) Investigation Experiment/Dynamics of the MJO (AMIE/DYNAMO) field campaign [Yoneyama *et al.*, 2013] and it has been a subject of several modeling studies [Hagos *et al.*, 2014a,b; Wang *et al.*, 2014; Janiga and Zhang, 2016; Powell, 2016]. The convection associated with this MJO event was initiated over the Indian Ocean on about 22 November and arrived at the MC at the beginning of December, where it stalled and weakened barely making it into the Pacific.

The model used in this study is the Weather Research and Forecasting (WRF) model [Skamarock *et al.*, 2008]. The details of the model setup are provided in Table 1 and the model domain is shown in Figure 1a. It covers the region between 20°S and 20°N and 90°E and 155°E. All simulations are run at 4 km grid spacing without a cumulus parameterization. In the control simulations (hereafter referred to as CONTROL), the top of the atmosphere (TOA) downwelling shortwave radiative flux ( $SW_{top}$ ) varies diurnally in the conventional manner (Figure 1b). In the other ensemble of simulations (hereafter NODC), the diurnal cycle in  $SW_{top}$  is removed by keeping  $SW_{top}$  constant at its daily mean value of roughly  $300 \text{ W m}^{-2}$  throughout the day. This flux varies with the seasonal solar cycle in both sets of simulations. Each ensemble has six members which are initialized on sequential days from 15–20 November. Lateral and surface boundary conditions are obtained from ERA-Interim reanalysis [Dee *et al.*, 2011] and are applied 6 hourly. Sea surface temperatures are prescribed and are applied 6 hourly as well. Extensive evaluations of the WRF model’s fidelity in capturing the initiation and propagation of MJO over the Indian Ocean and the simulated cloud populations are provided in Hagos *et al.* [2014a,b]. In this current study, we focus on model performance in representing observed aspects of MJO convection over the MC.

### 2.2. Observations

A number of observational data sets are used to evaluate the model simulations and to explore physical processes within the system. We use the precipitation estimates in the TRMM 3B42 data set [Huffman *et al.*, 2007], which are based on multispectral passive microwave and IR measurements, as the main target of MJO diagnostics. TRMM 3B42 has a 3 h temporal resolution and a spatial resolution of  $0.25^\circ \times 0.25^\circ$ . A geostationary-satellite-based  $11 \mu\text{m}$  infrared brightness temperature ( $T_b$ ) data set ([http://disc.sci.gsfc.nasa.gov/precipitation/data-holdings/Globally\\_merged\\_IR.shtml](http://disc.sci.gsfc.nasa.gov/precipitation/data-holdings/Globally_merged_IR.shtml)) is used to investigate the observed diurnal cycle of convective clouds between 20 October 2011 and 20 December 2011. The  $T_b$  data set has a native spatial resolution of approximately 4 km and updates every 1 h, which is comparable to that of the model simulations.

To examine the interactions between clouds and surface radiation, we use data collected at the Department of Energy (DOE) ARM site at Manus Island (2.06°S, 147.43°E) from January 2002 to December 2013. The various

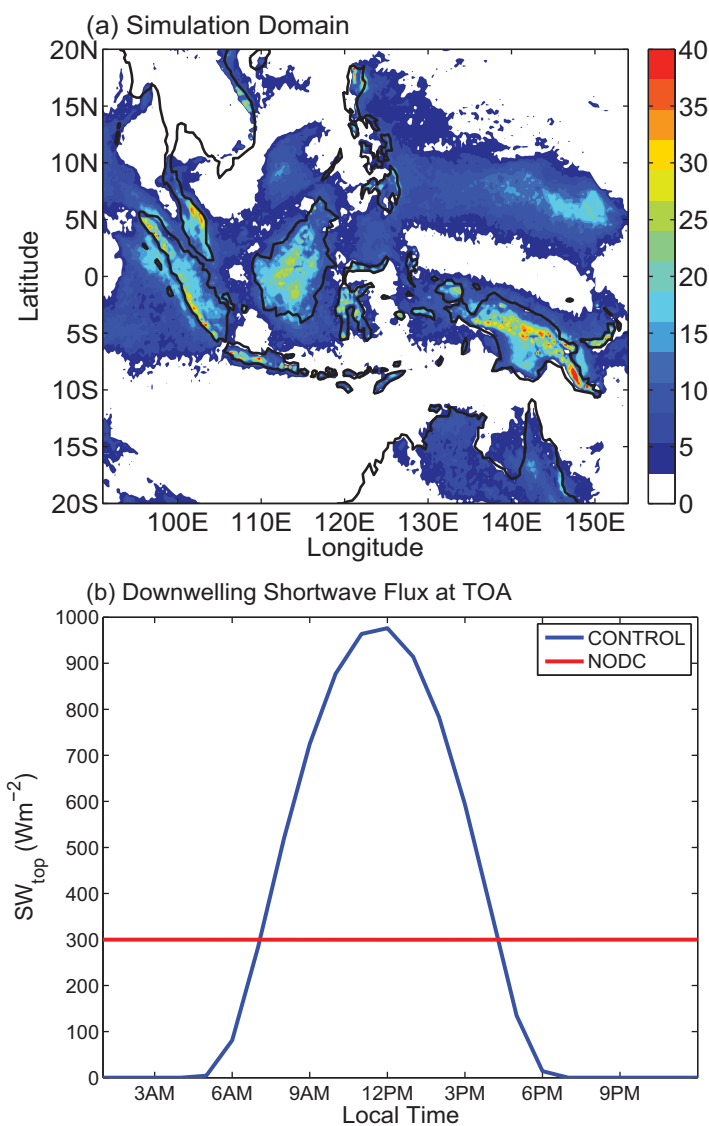


**Figure 1.** (a) Simulation domain and monthly mean precipitation from the model ( $\text{mm d}^{-1}$ ). (b) Top of the atmosphere (TOA) downwelling shortwave radiation ( $\text{W m}^{-2}$ ) for the CONTROL and NODC simulations averaged over the simulation period. The daily mean values are equal for the two simulations.

propagates across the MC and eventually diminished near  $150^\circ\text{E}$ . In the CONTROL simulations, in which precipitation is weaker than the observed over the eastern Indian Ocean, the eastward propagating signal ceases to exist past the MC. This is similar to the exaggerated barrier effect of MC in many numerical models. The weakening of the eastward propagating signal is much less severe in the NODC ensemble mean (Figure 2c) and the signal manages to move to the eastern edge of the MC. The effect of the diurnal cycle can be clearly seen in the difference between the two ensemble averages (Figure 2d). With the inclusion of the diurnal cycle, the propagating MJO signal is weakened while the standing signal over the islands of Sumatra and Borneo is enhanced.

To quantify the MC barrier effect in the CONTROL and NODC simulations, the Large-Scale Precipitation Tracking (LPT) [Kerns and Chen, 2016] metric has been applied to each simulation and to the TRMM data within the simulation domain using the same criteria as in Kerns and Chen [2016]: a  $5^\circ$  standard deviation Gaussian spatial filter applied to 3 day rain accumulations and a  $12 \text{ mm d}^{-1}$  feature threshold. For the spatial filter, the edge points of the regional domain were repeated as ghost points. Using the phase diagram representation of LPT as in Kerns and Chen [2016], the differences between the CONTROL and NODC simulations are evident (Figure 3). The CONTROL simulations reached amplitudes of  $\sim 1.5$  in the Maritime

data sets collected at Manus are described in Mather et al. [1998], Long et al. [2013], and McFarlane et al. [2013]. We use the measurements of cloudiness and downwelling shortwave radiative flux at the surface to derive estimates of the shortwave (SW) transmissivity, defined as the ratio of cloudy to clear-sky SW fluxes at the surface. SW transmissivity indicates the fraction of equivalent clear-sky SW fluxes that penetrate through the cloud and is not dependent on the solar zenith angle. In section 4, the observational data sets are grouped by MJO phases which are determined using the Real-Time Multivariate MJO (RMM) index [Wheeler and Hendon, 2004].

### 3. Results From the Model Simulations

#### 3.1. Impact of the Diurnal Cycle on Simulated Precipitation

We first consider the differences between the precipitation signals in CONTROL and NODC. The MC barrier effect on the MJO is illustrated in Figure 2, which shows the Hovmöller diagrams of precipitation from TRMM observations, the CONTROL and NODC simulations, and the difference between CONTROL and NODC. In the TRMM observations, the precipitation signal fluctuates as it

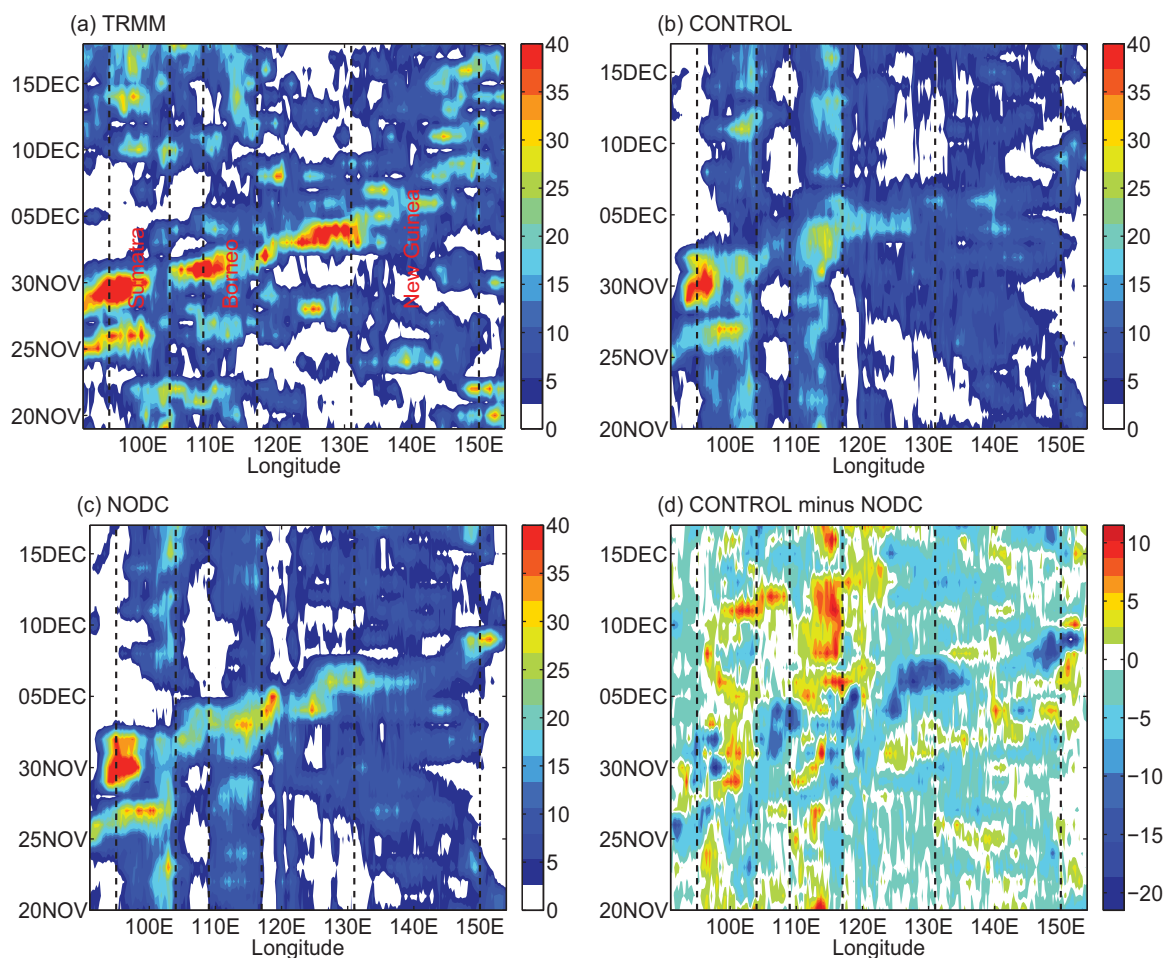


**Figure 2.** Hovmöller diagrams of precipitation ( $\text{mm d}^{-1}$ ) averaged between  $5^{\circ}\text{S}$  and  $5^{\circ}\text{N}$  from (a) TRMM, (b) CONTROL, (c) NODC, and (d) the difference between CONTROL and NODC. The vertical dashed lines mark the boundaries of the islands of Sumatra, Borneo, and New Guinea.

Continent but stagnated there and did not reach the west Pacific. In contrast, the NODC simulations showed a robust eastward propagation across the Maritime Continent to phase 6 with amplitudes of  $\sim 2$  (e.g., 1200 km effective radius). While none of the simulations reproduced the amplitude of the TRMM LPT, this study focuses on the weakening of the precipitation signal and the much greater MC barrier effect in the CONTROL simulations.

The weakening of the propagating precipitation signal is apparent not only over the interisland seas of the MC, but also over the eastern Indian Ocean as well as over the islands themselves. In CONTROL, the precipitation over the islands of Sumatra and Borneo is enhanced just ahead of the arrival of the MJO convection. The enhancement of precipitation signal over the islands ahead of the MJO convection is consistent with the observations of Peatman *et al.* [2014]. This is apparent in its time series over land (including Sumatra and Borneo) and ocean separately, averaged over a box of  $5^{\circ}\text{S}$ – $5^{\circ}\text{N}$  and  $95^{\circ}\text{E}$ – $120^{\circ}\text{E}$  (Figure 4). When the MJO convection signal is over the Indian Ocean (20–22 November), the diurnal cycle briefly enhances precipitation over the islands (CONTROL in Figure 4a). However, upon the arrival of the MJO (22 November to 2 December), precipitation over the islands is weakened. After this time, the diurnal cycle of solar insolation enhances precipitation over the islands in the CONTROL ensemble mean compared to the NODC ensemble mean. Over the ocean, the CONTROL simulations have weaker precipitation when the MJO convection crosses the MC (27 November to 9 December; Figure 4b). Thus, the diurnal cycle modulates the variation of precipitation by enhancing the standing local precipitation over the islands and weakening the oceanic precipitation propagating over the surrounding seas and to the Pacific as part of the MJO signal. A combination of these two effects results in the apparent stalling of the MJO convection over the MC in CONTROL.

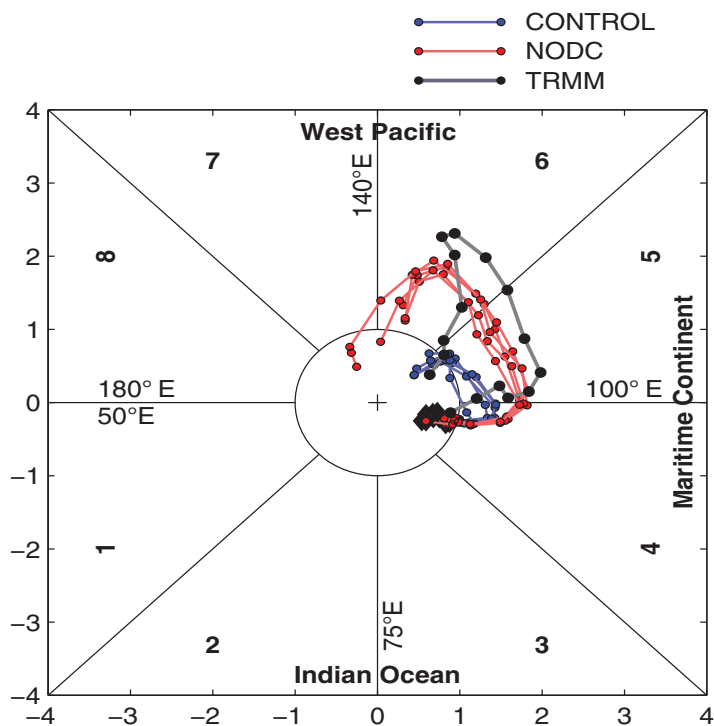


**Figure 3.** Large-scale precipitation tracking (LPT) phase diagram for 24 November to 22 December 2011 for TRMM (black), the CONTROL simulations (blue), and the NODC simulations (red). The circle markers are for daily mean LPT longitude and amplitude. Diamonds indicate the LPT initiation points. LPT phase is determined by the longitude of the centroid of convection with breakpoints indicated on the diagram. Amplitude is the effective radius divided by 600 km. Only the longest lasting LPTs within the model simulation domain for TRMM and for each simulation are drawn.

### 3.2. The Role of the Diurnal Cycle of Cloudiness

In order to understand the cause of the stalled precipitation over the islands in the presence of the solar diurnal cycle, we examine the time series of daily mean downwelling shortwave radiation at the surface ( $SW_{sfc}$ ; Figure 5a). On average, the mean  $SW_{sfc}$  in CONTROL is larger than that in NODC even though, by design, the daily mean  $SW_{top}$  are the same in both sets of simulations. This suggests that the diurnal cycle of cloudiness in the simulations significantly modulates the net  $SW_{sfc}$ . This becomes clear if one considers diurnal cycle of  $T_b$  over the islands of Sumatra and Borneo. Figures 5b and 5c show time-longitude diagrams of ensemble mean  $T_b$  in the CONTROL and NODC simulations. In CONTROL (Figure 5b), convection over the islands begins in the midafternoon, well after the peak of  $SW_{sfc}$ . In NODC (Figure 5c), cloudiness is roughly constant except for the small variations associated with the diurnal cycle of SST forcing (SSTs are prescribed from observations in both CONTROL and NODC and thus have a small diurnal cycle). The behavior is manifested in Figure 5d, where the observed diurnal cycle of precipitation is fairly well represented by the CONTROL simulation but essentially absent in the NODC ensemble (by design). In the CONTROL simulations, relatively clear skies persist in the window between sunrise and early afternoon after which clouds develop. These clear skies in the morning allow more shortwave radiation to reach the surface in CONTROL compared to NODC, which is equally cloudy across the diurnal cycle.

The effect of the diurnal cycle of cloudiness on  $SW_{sfc}$  and hence on precipitation over the islands of the MC, can be quantified by considering  $SW_{sfc}$  in a hypothetical situation in which clouds are randomly distributed in time within a day. In other words, what would the surface downwelling shortwave radiation be if the clouds from the CONTROL simulation randomly occurred at any time of the day instead of preferentially occurring in the afternoon? The daytime effect of clouds can be calculated by comparing the cloudy and clear-sky radiative fluxes. However, in order to assess the effect of random cloudiness one needs to be able to account for the effective transmissivity of clouds not only during daytime, but also at night. To that end, we examine the relationship between the daytime transmissivity of clouds and precipitation in both the simulations and observations. Figure 6a shows this relationship derived from our simulations. The correlation coefficient between transmissivity and surface rain rate is  $-0.58$ , which is statistically significant at 95% confidence level, suggesting a more or less linear relationship. We use this statistical relationship to infer the effective “nighttime transmissivity” of clouds occurring at night.

Using the directly calculated daytime transmissivities along with the derived nighttime transmissivity values, we estimate the total transmissivity across the diurnal cycle associated with a time series of “random clouds.” In the “random clouds” time series, the amount of clouds occurring in the day is kept the same but their time of occurrence is randomly selected from the 24 h of the day. The randomly redistributed

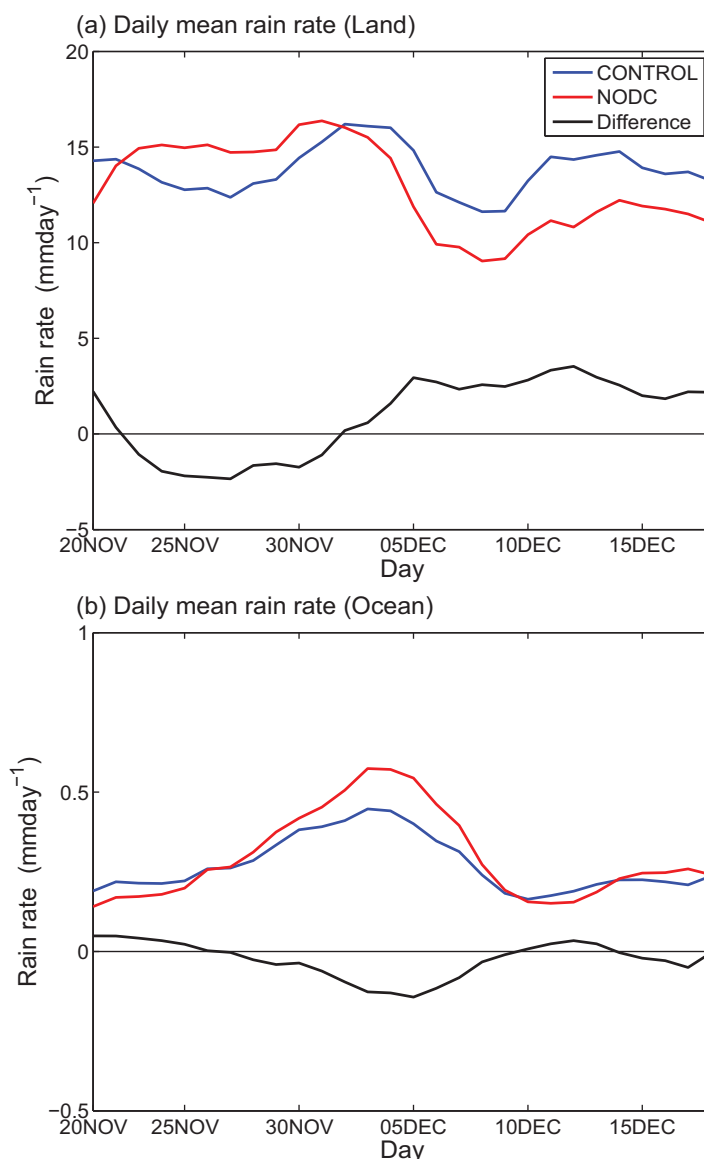


**Figure 4.** Daily mean rain rate averaged over (a) the islands of Sumatra and Borneo and (b) the adjacent waters. The averaging areas are 95°E–120°E and 5°S–5°N and the time series are smoothed by a 5-point moving average.

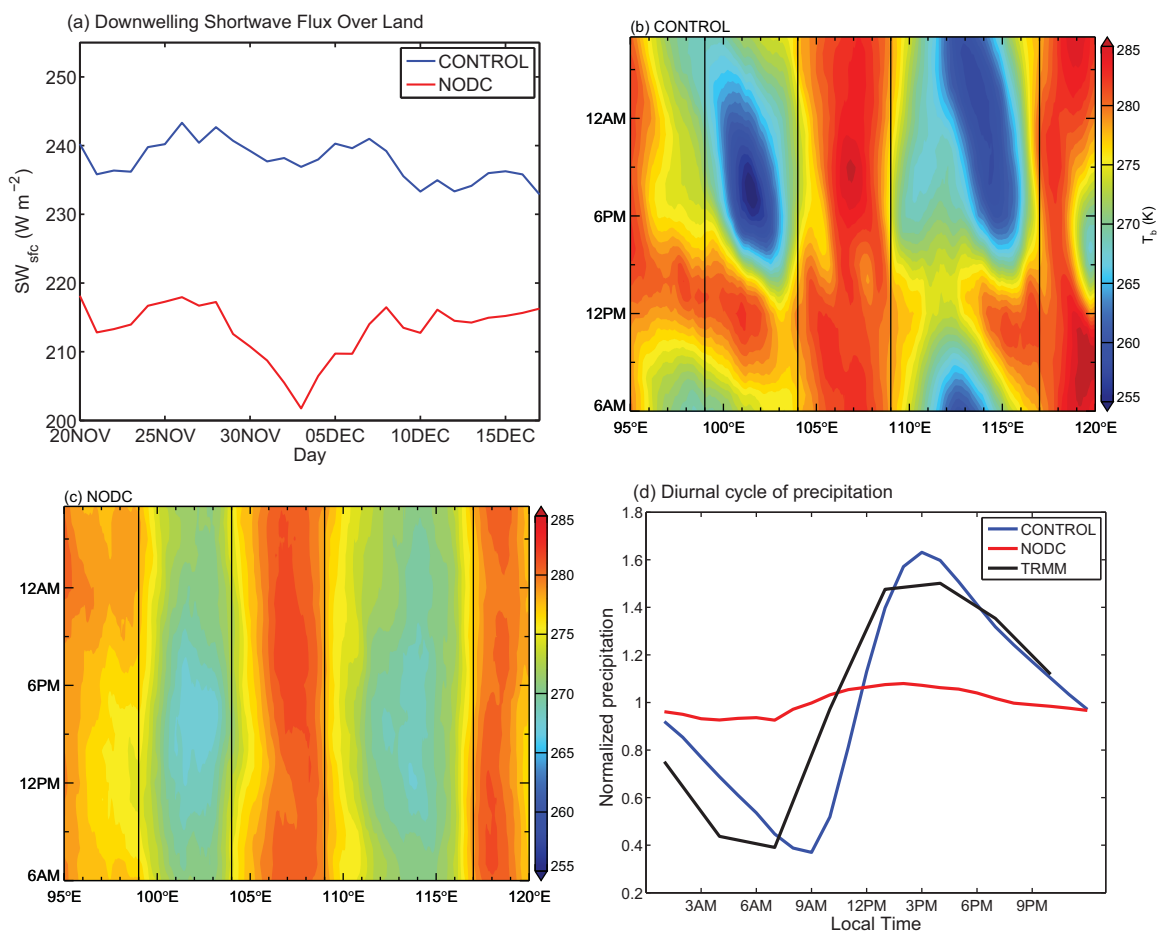
between CONTROL and NODC. This implies that up to 34% of the total difference has to be related to differences in the size and lifetime of the simulated clouds. To quantify these differences, the convective clouds in the two sets of simulations are tracked using the cloud-tracking algorithm described by *Feng et al.* [2012] and *Hagos et al.* [2013]. Individual cloud systems with a contiguous region of  $T_b$  colder than 260 K are identified and tracked throughout their lifetime. We use a relatively warm brightness temperature threshold for tracking in order to capture nonprecipitating anvil cloud shields associated with precipitating deep convection, since anvil clouds cover much larger area and dominate the cloud radiative effects [*Feng et al.*, 2011, 2012]. Given the hourly output of the simulation and satellite observations, only cloud systems with a lifetime of 3 h or longer are identified and tracked.

Figure 7 shows the distributions of land initiated cloud system lifetime, cloud system size (maximum effective radius), and total accumulated cloud area with respect to maximum cloud radius. Maximum effective radius, calculated as  $\sqrt{Area_{max}/\pi}$ , is obtained during each cloud system's lifetime. Total accumulated cloud area is cloud area integrated over each tracked cloud system's lifetime. The six ensemble simulations of 1

transmissivity values (i.e., random clouds) are then applied to the actual diurnally varying  $SW_{top}$  from CONTROL simulations to estimate what  $SW_{sfc}$  would be in the absence of a diurnal cycle of cloudiness. Figure 6b shows the daily mean  $SW_{sfc}$  from CONTROL, NODC, as well as the “random clouds” calculation. The difference between CONTROL and the “random clouds” calculation is roughly 66% of the difference between CONTROL and NODC. In other words, 66% of the difference of  $SW_{sfc}$  between CONTROL and NODC comes from clouds over the islands that preferentially form during the afternoon in the CONTROL ensemble. The relatively clear-sky conditions preceding this afternoon cloud development allow more short-wave radiation to reach the surface compared to the scenario where clouds randomly formed at any time of the day, which is the case in NODC. This “random clouds” method of quantifying the role of the diurnal cycle of cloudiness will be applied to observations in section 4.

### 3.3. Impact of the Diurnal Cycle on Cloud System Characteristics

As noted in the discussion above, the diurnal cycle of cloudiness accounts for roughly 66% of the difference in  $SW_{sfc}$



**Figure 5.** (a) Diurnal mean surface downwelling shortwave radiation (SWsfc) averaged over the islands of Sumatra and Borneo and smoothed by a 5-point moving average, Hovmöller diagram of diurnal cycle of outgoing infrared brightness temperature ( $T_b$ ) from (b) CONTROL and (c) NODC averaged between 5°S and 5°N. (d) Diurnal cycle of precipitation averaged over Sumatra and Borneo, normalized by the daily mean.

month each in both CONTROL and NODC collectively produce a larger sample size than the satellite data set, which is 2 months long. For direct comparison, the total number of cloud systems in the observations is artificially scaled (multiplying by approximately 3) to match the sample size of clouds in the simulations. This scaling changes the absolute counts of cloud systems in the observations, but retains their distribution. The number distributions of cloud systems in the two sets of simulations follow an exponential decrease with increasing lifetime and generally agree with the observations (Figure 7a). The maximum cloud system sizes from the simulations are slightly smaller compared to the satellite observations, with the simulated peaks at 30–40 km compared to the observed peak at 50 km (Figure 7b).

Clouds that initiate in the afternoon influence the surface downwelling shortwave radiation during the first 6 h of their lifetime (before dusk). In CONTROL, the majority of clouds are initiated in the afternoon and they are relatively small before sunset and hence allow more shortwave radiation to reach the surface. In contrast, there is no preferential diurnal timing of clouds in the NODC simulations and since the sun is shining all the time, clouds of any size and lifetime can block the shortwave radiation from reaching the surface. This is shown in the comparison of the distribution of cloud system lifetime shows that NODC simulations have substantially more short-lived (<6 h) clouds than the CONTROL simulations (Figure 7a). As a result, the NODC simulations produce more small clouds (maximum radius <70 km) and less large clouds than CONTROL simulations (Figure 7b). This is not surprising because the forcing in the NODC is uniform in time and hence one expects less spread in cloud characteristics. Furthermore, the perpetual morning favors the formation of more clouds that do not last as long or grow as large. On the other hand, the diurnal cycle of solar insolation favors fewer but longer lasting clouds because the formation of new clouds would be suppressed at night and strong surface heating in the afternoon would favor the growth and longevity of the clouds that are formed.

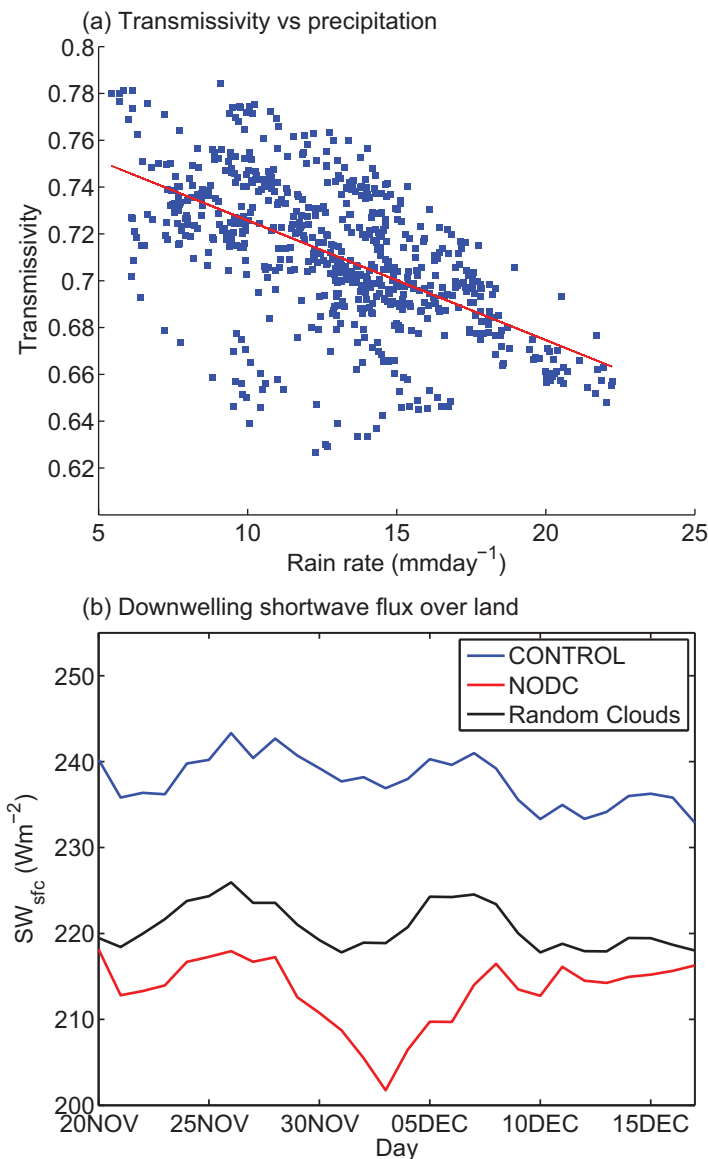


**Figure 6.** (a) Relationship between rain rate and transmissivity from the CONTROL simulation. The correlation is  $-0.58$ , (b) as in Figure 4a, but including diurnal mean surface downwelling shortwave radiation using the hypothetical random diurnal distribution of cloudiness.

how surface heat fluxes, winds, and temperature over land respond to diurnal variations of  $SW_{sfc}$ . Figures 8a–8c show the mean time series of these variables for the CONTROL and NODC ensembles. As expected from an energy balance perspective, the sum of latent and sensible fluxes over the islands in CONTROL is larger by  $22 \text{ W m}^{-2}$  compared to the NODC ensemble. The daily mean wind speeds are comparable. However, the land surface is cooler in CONTROL by about 1 K. Given the larger surface downwelling radiation, the cooler land surface in CONTROL is counterintuitive. To understand this, we consider the diurnal cycles of surface (10 m) wind speed and surface skin temperature (Figure 8d). They more or less covary in CONTROL, with surface wind speed reaching its peak within 2 h of peak surface temperature (noon). That means the diurnal cycle in CONTROL cools the land surface very efficiently by ventilating it when it is warm. In NODC however, by design, neither variable has a diurnal cycle therefore the covariance is essentially zero. Hence, the turbulent fluxes are not as efficient in transferring heat away from the surface. This difference represents the rectification of diurnal temperature fluctuations into low-frequency variability by eddy flux divergence and is similar to the multiscale process proposed by *Majda and Yang* [2016] to explain the

Since short-lived cloud systems are more important to surface shortwave radiation as discussed above, we examine the total accumulated cloud area for cloud systems lasting no longer than 6 h as a function of maximum cloud radius. Figure 7c shows that total cloud area in NODC simulations are larger than CONTROL simulations for small clouds (maximum radius  $<70 \text{ km}$ ). The increased cloud area from larger clouds in the CONTROL simulations is not sufficient to overcome this difference because much of it happens at night. Thus, in addition to the diurnal cycle of cloudiness discussed in the last section, more short-lived cloud systems in the NODC simulations lead to less surface downwelling shortwave radiation compared to the CONTROL simulations (Figures 6b and 7c). Such differences in the size and lifetime of clouds between the two sets of simulations essentially explain the remaining 34% difference in the randomized cloud experiment discussed in Figure 6b.

### 3.4. Impact of the Diurnal Cycle on Land Surface Processes

In the last two subsections, the mechanisms through which the diurnal cycle of cloudiness affects  $SW_{sfc}$  were examined. In this subsection, we investigate

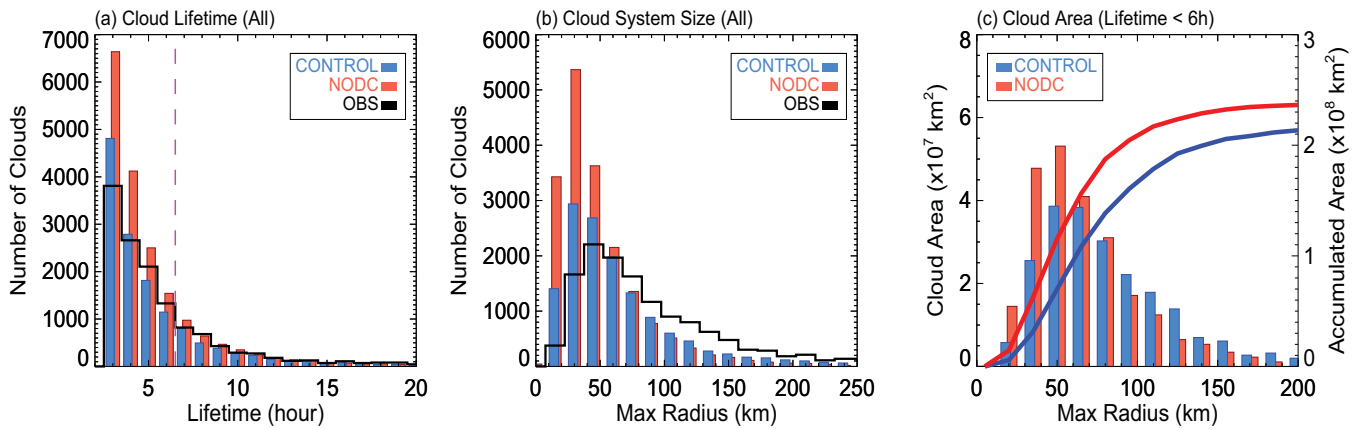


**Figure 7.** Statistics of convective cloud systems initiated over land: (a) lifetime of clouds, (b) maximum equivalent radii of clouds during their lifetime, and (c) total integrated maximum cloud area for each radius bin (number of cloud systems in each radius bin  $\times$  radius value). Cloud systems include all clouds with infrared brightness temperature lower than 260 K. The vertical dashed line in Figure 7a marks lifetime of 6 h.

weakening of the diurnal cycle over the MC by the MJO. It likely has important implications for other processes such as the Hadley circulation and land-sea contrasts in monsoons and should be investigated further.

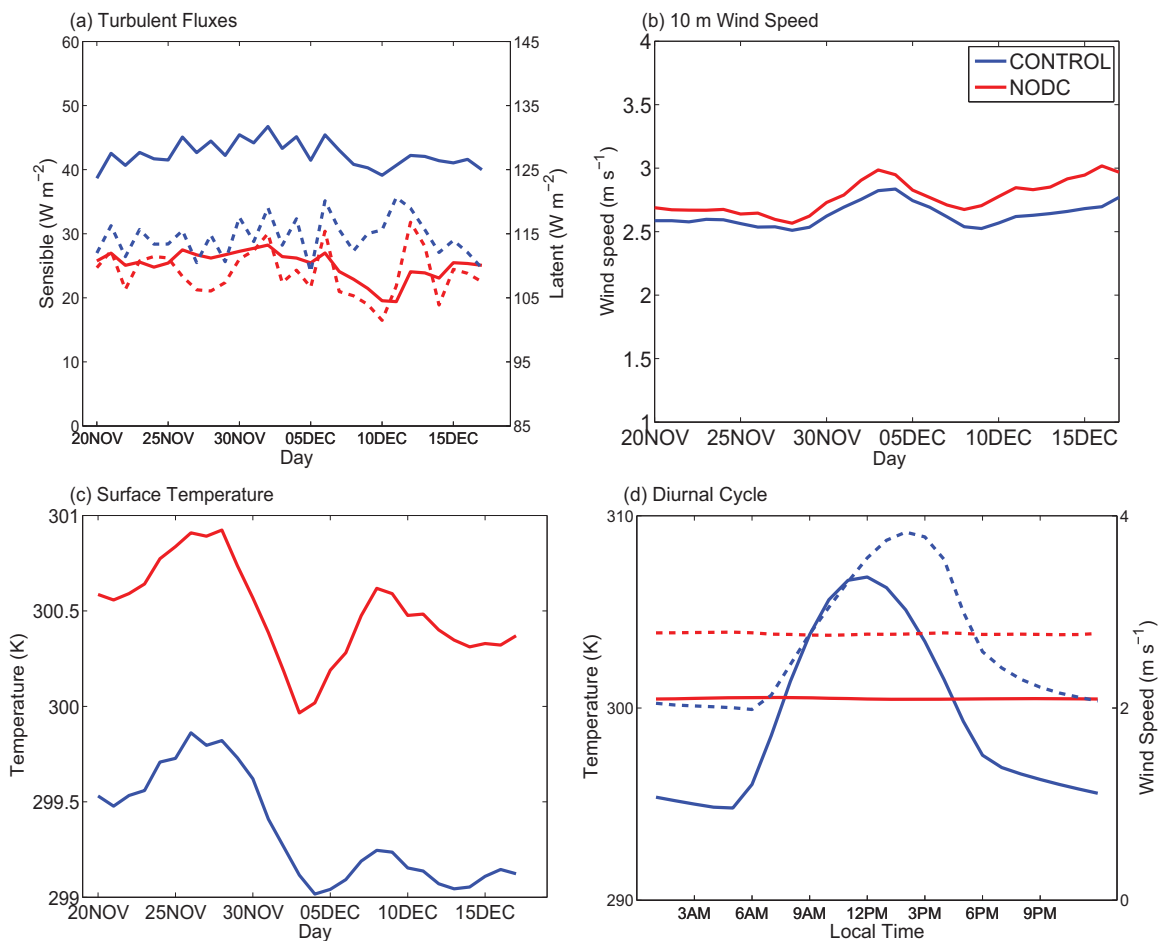


**Figure 8.** Time series of diurnal mean surface sensible (solid) and latent (dashed) heat flux, (b) 10 m wind speed, (c) land surface temperature, and (d) monthly mean diurnal cycles of surface skin temperature (solid) and 10 m wind speed (dashed). CONTROL ensemble mean is in blue and NODC ensemble mean is in red. All are averaged over the Islands of Sumatra and Borneo and the time series in Figures 8a–8c are smoothed by a 5-point moving average.

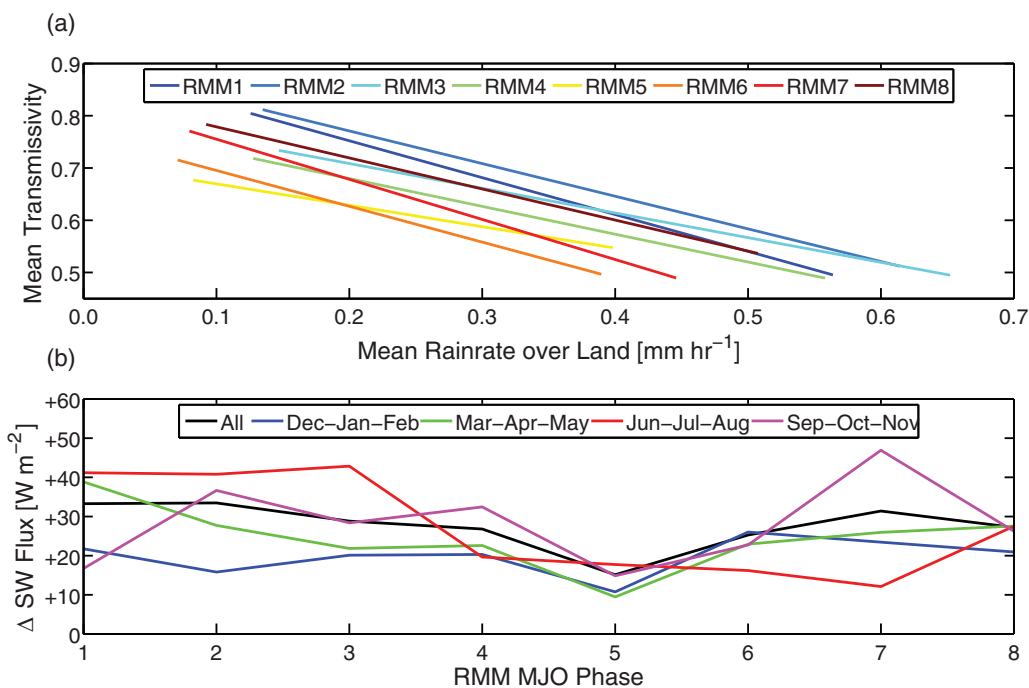


**Figure 9.** (a) Linear-regression relationship between the mean rain rate over land in the MC and the mean SW transmissivity (the ratio of cloudy to clear-sky SW flux at the surface) at the Manus DOE ARM site. (b) Change in the total SW flux reaching the surface that would occur if the observed clouds were randomly distributed across the diurnal cycle. The regressions and change in SW flux are both derived for each RMM MJO phase. Black is for all year and the colors are for different seasons.

#### 4. Analysis of Observations

The “random clouds” experiment described in section 3b demonstrated that the diurnal cycle of cloudiness increases the total amount of solar radiation reaching the surface. In the hypothetical situation in which clouds are randomly distributed throughout the day, mean  $SW_{sfc}$  decreased by about  $20 \text{ W m}^{-2}$ , or roughly 66% of the total difference between the CONTROL and NODC ensembles. In this section, we examine the impact of diurnal cycle of cloudiness on surface downwelling shortwave radiation and how it varies with MJO phase using the ARM observations collected on the island of Manus ( $2.06^\circ\text{S}$ ,  $147.425^\circ\text{E}$ ) in the MC. The ARM transmissivity measurements and the measured rain rates over land from the TRMM 3B42 precipitation product are used to derive a statistical relationship between the mean rain rate over land and mean SW transmissivity for each of the eight RMM MJO phases. Hourly mean SW transmissivity values are paired with the mean rain rate over land which was computed in a  $10^\circ$  diameter box centered on Manus. The mean rain rate data are interpolated from 3 h resolution to 1 h resolution to match the radiation data. The correlations between the mean rain rate over land and SW transmissivity at Manus ranged from  $-0.83$  to  $-0.96$  (Figure 9a), indicating a strong and reliable relationship. All correlations are statistically significant at the 99% confidence level. These derived relationships are then used to perform a “random clouds” experiment for each MJO phase in the same manner as the simulations (section 3b).

The mean changes in  $SW_{sfc}$  from the observational control (i.e., the original data set) and the “random clouds” experiment for each MJO phase are shown in Figure 9b. The difference between the actual  $SW_{sfc}$  and that with randomized clouds ranges from approximately  $+34 \text{ W m}^{-2}$  (MJO Phases 1 and 2) to  $+15 \text{ W m}^{-2}$  for MJO Phase 5, when the MJO convective envelope is over Manus. The magnitudes of the change are similar to those derived from the simulations and are strongly related to the amplitude of the precipitation diurnal cycle over the islands of the MC. The smaller impact during MJO Phase 5 reflects the increase in cloudiness at all times of the day during the active phase of the MJO. In other words, because total cloudiness over the MC is increased due to the MJO convectively active phase, the amplitude of the cloudiness diurnal cycle is suppressed and thus randomizing the clouds across the diurnal cycle has a smaller impact. The impact of the diurnal cycle of cloudiness is largest during the suppressed phases of the MJO (MJO Phases 1 and 2), when clear skies enhance solar heating of the surface before the afternoon cloud development, leading to a larger amplitude diurnal cycle of precipitation over land.

The varying importance of the diurnal cycle of solar radiation by MJO phase (i.e., the impact of the “random clouds” experiment) demonstrates that the diurnal cycle is not only modulated by the MJO, but also feeds back onto the propagation of the MJO as it crosses the MC. During a suppressed phase of the MJO, the diurnal cycle of cloudiness allows for up to  $34 \text{ W m}^{-2}$  of  $SW_{\text{sfc}}$  enhancement, which in turn promotes more frequent convection over land ahead of the main MJO convective envelope. This effect is suppressed as the MJO crosses the MC because cloudiness is increased at all times of the day and a smaller amplitude diurnal cycle of surface heating is less favorable for convection over land. As the MJO exits the MC, the amplitude of the diurnal cycle increases and the subsequent enhancement of  $SW_{\text{sfc}}$  again favors convection over land. The enhancement of convection over the islands of the MC ahead of and behind an active phase of the MJO disrupts the smooth propagation of the MJO and leads to the stalling and weakening of the MJO signal over the MC. This effect of the diurnal cycle varies by season as the TOA downwelling shortwave radiation on which the clouds are acting is larger in summer (Figure 9b). This is consistent with the *Kerns and Chen* [2016] finding that the weakening of propagating MJO convection signals is more frequent in late summer/early autumn compared to the winter. Their study also shows that the propagation of MJO convection across the MC is more likely to be blocked during the El-Niño phase of ENSO, as one would expect since reduced cloudiness and therefore increased insolation over the MC are favorable conditions for the process we discuss in this paper.

## 5. Summary and Conclusions

This study examines the impact of the diurnal cycle on the propagation of MJO convection across the MC. The motivation of the study is the peculiar and largely unpredictable behavior of MJO propagation across the MC. Previous studies have noted that convective activity over the islands of the MC is usually enhanced just ahead of the arrival of the main convection envelope of the MJO that propagates through the MC but often weakens over the large islands of Sumatra, Borneo, and New Guinea [*Peatman et al.*, 2014]. On the other hand, some MJO events fail to propagate across the MC. Such variation in MJO propagation across the MC cannot be explained just by the presence of topography and land-sea contrasts, which affect all MJO episodes in the same manner. In this study, both simulations and observations are used to examine the role of the diurnal cycle of surface insolation, which can be modulated by the MJO and perhaps other modes of low-frequency variability.

A pair of ensemble simulations with six members each is performed. In the CONTROL ensemble, the incoming shortwave radiation at the top of the atmosphere ( $SW_{\text{top}}$ ) varies diurnally as in nature while in the NODC this diurnal cycle is replaced by  $SW_{\text{top}}$  fixed at the daily mean value throughout the day. In the CONTROL ensemble, the solar diurnal cycle enhances precipitation over the large islands in the MC and the propagating MJO precipitation signal is weak. Without the solar diurnal cycle, the propagating MJO signal is enhanced over the MC in the NODC. Surface daily mean downwelling shortwave radiation over the islands is larger in the CONTROL than in the NODC ensemble, even though the daily mean  $SW_{\text{top}}$  is the same in both. This is related to the fact that in the presence of the solar diurnal cycle, cloudiness peaks well after the peak downwelling shortwave radiation (local noon) giving plenty of time for the surface to receive a large amount of solar radiation under relatively clear-sky conditions before cloud development in the afternoon. A hypothetical scenario where clouds in the CONTROL are randomly distributed throughout the day reveals that up to 66% of the difference in downwelling surface shortwave radiation between CONTROL and NODC comes from the effect of the diurnal cycle of cloudiness. The rest is related to the fact that there are more short-lived small cloud systems in the NODC simulations, particularly during late morning to early afternoon when downwelling shortwave radiation peaks, resulting in more cloudiness and less surface downwelling shortwave radiation than in the CONTROL simulations. Analysis of the land surface processes in the two sets of simulations indicates that phase relationships between the diurnal cycles of surface wind speed and skin temperature in CONTROL favor enhanced heat fluxes that cool the land surface by about 1 K compared to NODC.

The mechanism inferred from the analysis of the simulations is verified using observations. Long-term radiative flux observations from the DOE ARM site at Manus and precipitation from TRMM 3B42 data product are used to derive statistical relationships between cloud shortwave transmissivity and precipitation over land for each of the eight RMM MJO phases. In a manner similar to the diagnostics of the model simulations, the

impact of the diurnal cycle on surface shortwave radiation is estimated by comparing the observations to calculations with cloudiness (transmissivity) randomly distributed throughout the day. We find that the diurnal cycle of cloudiness introduces an extra +15 to +34 W m<sup>-2</sup> of downwelling shortwave radiation at the surface, comparable to the estimates based on the simulations. The effect of the diurnal cycle on downwelling shortwave radiation is out of phase with the MJO, such that it is stronger before and after an MJO active phase crosses over the MC (RMM MJO Phases 4 and 5) and hence disrupts the smooth propagation of the MJO signal as demonstrated in the model simulations. These results are in agreement with the modeling study of *Birch et al.* [2016], who also found that rainfall peaks before the main convective envelope arrives due to strong convective triggers from high surface insolation and surface heating. On the other hand, during the peak MJO phases they find that cloud cover increases and surface insolation decreases.

The reason that enhanced diurnal cycle over land would disrupt the propagation of the MJO stems from the competition between convection over the islands and the surrounding seas in the MC. The main convective signal of the MJO propagating through the MC is over its seas. The standing convection over the islands enhanced by the diurnal cycle is almost synchronized over the entire MC. It competes with convection over the surrounding waters through land-sea breezes and moisture supply. In our simulations, when the MJO failed to propagate through the MC in the CONTROL, convection over the islands dominates that over the surrounding waters. When the propagating signal of the MJO over the MC is strengthened without the diurnal cycle in the NODC, convection over the waters dominates that of the islands in the MC.

In summary, the modulation of downwelling shortwave radiation by the diurnal cycle of cloudiness may play a large role in causing convection of the MJO to stall over the large islands of the MC at the expense of the propagating MJO convection signal. This might not be the only mechanism through which the MC islands affect MJO propagation across the MC; their topography and land surface heterogeneity could as well be very important. Nonetheless, this study presents a potential mechanism by which large-scale low-frequency variabilities can affect the MJO propagation through their modulation of the diurnal cycle in cloudiness. The effect of diurnal cycle of cloudiness varies by season and it is strongest during boreal summer, when the weakening of propagating MJO convection signals is more frequent [*Kerns and Chen*, 2016]. Thus, our study could also help explain why some MJO events overcome the MC barrier while others do not. The potential influences of interannual variability (e.g., ENSO, QBO, monsoons, etc.) on MJO propagation via this and other mechanisms are subjects of an ongoing research and will be reported in the future.

#### Acknowledgments

This research was supported by the U.S. Department of Energy Office of Science Biological and Environmental Research as part of the Atmospheric Systems Research Program and Regional and Global Climate Modeling Programs (authors S.H., C.B., Z.F., and M.M.) and a NOAA CPO grant NA13OAR4310161 (author C.Z.). Data from the U.S. Department of Energy's Atmospheric Radiation Measurement (ARM) Climate Research Facility Manus site are used. Computing resources for the model simulations are provided by the National Energy Research Scientific Computing Center (NERSC). Pacific Northwest National Laboratory is operated by Battelle for the U.S. Department of Energy under contract DE-AC05-76RLO1830.

#### References

- Birch, C. E., S. Webster, S. C. Peatman, D. J. Parker, A. J. Matthews, Y. Li, and M. E. E. Hassim (2016), Scale Interactions between the MJO and the Western Maritime Continent, *J. Clim.*, *29*, 2471–2492.
- Dee, D., et al. (2011), The ERA-Interim reanalysis: Configuration and performance of the data assimilation system, *Quart. J. Roy. Meteor. Soc.*, *137*, 553–597.
- Feng, Z., X. Q. Dong, B. K. Xi, C. Schumacher, P. Minnis, and M. Khaiyer (2011), Top-of-atmosphere radiation budget of convective core/stratiform rain and anvil clouds from deep convective systems, *J. Geophys. Res.*, *116*, D23202, doi:10.1029/2011JD016451.
- Feng, Z., X. Q. Dong, B. K. Xi, S. A. McFarlane, A. Kennedy, B. Lin, and P. Minnis (2012), Life cycle of midlatitude deep convective systems in a Lagrangian framework, *J. Geophys. Res.*, *117*, D23201, doi:10.1029/2012JD018362.
- Hagos, S., Z. Feng, S. McFarlane, and L. R. Leung (2013), Environment and the lifetime of tropical deep convection in a high resolution regional model simulation, *J. Atmos. Sci.*, *70*(8), 2409–2425.
- Hagos, S., Z. Feng, K. Landu, and C. N. Long (2014a), Advection, moistening, and shallow-to-deep convection transitions during the initiation and propagation of Madden-Julian Oscillation, *J. Adv. Model. Earth Syst.*, *6*, 938–949, doi:10.1002/2014MS000335.
- Hagos, S., Z. Feng, C. Burleyson, K.-S. Lim, C. N. Long, D. Wu, and G. Thompson (2014b), Evaluation of high resolution simulations of cloud populations in Madden-Julian oscillation using data collected during AMIE/DYNAMO field campaign, *J. Geophys. Res. Atmos.*, *119*, 12,052–12,068, doi:10.1002/2014JD022143.
- Hagos, S. M., Z. Feng, C. D. Burleyson, C. Zhao, M. N. Martini, and L. K. Berg (2015), Moist process biases in simulations of the Madden-Julian Oscillation episodes observed during the AMIE/DYNAMO field campaign, *J. Clim.*, *29*, 1091–1077, doi:10.1175/JCLI-D-15-0349.1.
- Hong, Y. N., and J. Dudhia (2006), A new vertical diffusion package with explicit treatment of entrainment processes, *Mon. Weather Rev.*, *134*, 2318–2341.
- Hsu, H.-H., and M. Y. Lee (2005), Topographic effects on the eastward propagation and initiation of the Madden-Julian oscillation, *J. Clim.*, *18*, 795–809.
- Huffman, G. J., et al. (2007), The TRMM multi-satellite precipitation analysis: Quasi-global, multi-year, combined-sensor precipitation estimates at fine scale, *J. Hydrometeorol.*, *8*, 38–55, doi:10.1175/JHM560.1.
- Janiga, M. A., and C. Zhang (2016), MJO moisture budget during DYNAMO in a cloud-resolving model, *J. Atmos. Sci.*, *73*, 2257–2277, doi:10.1175/JAS-D-14-0379.1.
- Jiang, X., et al. (2015), Vertical structure and physical processes of the Madden-Julian oscillation: Exploring key model physics in climate simulations, *J. Geophys. Res. Atmos.*, *120*, 4718–4748, doi:10.1002/2014JD022375.

- Kerns, B. W., and S. S. Chen (2016), Large-scale precipitation tracking and the MJO over the Maritime Continent and Indo-Pacific warm pool, *J. Geophys. Res. Atmos.*, *121*, 8755–8776, doi:10.1002/2015JD024661.
- Kim, D., K. Sperber, W. Stern, D. Waliser, I. Kang, E. Maloney, W. Wang, K. Weickmann, J. Benedict, and M. Khairoutdinov (2009), Application of MJO simulation diagnostics to climate models, *J. Clim.*, *22*(23), 6413–6436.
- Long, C. N., et al. (2013), ARM research in the equatorial western Pacific: A decade and counting, *Bull. Am. Meteorol. Soc.*, *94*, 695–708, doi:10.1175/BAMS-D-11-00137.1.
- Majda, A. J., and Q. Yang (2016), A multi-scale model for the intraseasonal impact of the Diurnal Cycle over the Maritime Continent on the Madden-Julian oscillation, *J. Atmos. Sci.*, *73*(2), 579–604.
- Mather, J. H., T. P. Ackerman, W. E. Clements, F. J. Barnes, M. D. Ivey, L. D. Hatfield, and R. M. Reynolds (1998), At atmospheric radiation and cloud station in the tropical western Pacific, *Bull. Am. Meteorol. Soc.*, *79*, 627–642, doi:10.1175/1520-0477(1998)079 <0627:AAR-ACS>2.0.CO;2.
- McFarlane, S. A., C. N. Long, and J. Flaherty (2013), A climatology of surface radiative effects at the ARM tropical western Pacific sites, *J. Appl. Meteorol. Climatol.*, *52*, 996–1013, doi:10.1175/JAMC-D-12-0189.1.
- Mlawer, E. J., S. J. Taubman, P. D. Brown, M. J. Iacono, and S. A. Clough (1997), Radiative transfer for inhomogeneous atmosphere: RRTM, a validated correlated-k model for the longwave, *J. Geophys. Res.*, *102*(D14), 16,663–16,682.
- Morcrette, J. J., et al. (2008), Impact of a new radiation package, McRad, in the ECMWF integrated forecasting system, *Mon. Weather Rev.*, *136*(12), 4773–4798.
- Neena, J. M., J.-Yi Lee, D. Waliser, B. Wang, and X. Jiang (2014), Predictability of the Madden-Julian Oscillation in the Intraseasonal Variability Hindcast Experiment (ISVHE), *J. Clim.*, *27*, 4531–4543.
- Peatman, S., A. Matthews, and D. P. Stevens (2014), Propagation of the Madden-Julian Oscillation through the Maritime Continent and scale interaction with the diurnal cycle of precipitation, *Q. J. R. Meteorol. Soc.*, *140*, 814–825.
- Powell, S. W. (2016), Updraft buoyancy within and moistening by cumulonimbi prior to MJO convective onset in a regional model, *J. Atmos. Sci.*, *73*, 2913–2934, doi:10.1175/JAS-D-15-0326.1.
- Rauniyar, P., and K. Walsh (2011), Scale interaction of the diurnal cycle of rainfall over the Maritime Continent and Australia: influence of the MJO, *J. Clim.*, *24*, 325–348.
- Rui, H., and B. Wang (1990), Development characteristics and dynamic structure of tropical intraseasonal convection anomalies, *J. Atmos. Sci.*, *47*, 357–379.
- Salby, M. L., and H. H. Hendon (1994), Intraseasonal behavior of clouds, temperature and motion in the tropics, *J. Atmos. Sci.*, *51*, 2207–2224.
- Seo, K.-H., W. Wang, J. Gottschalck, Q. Zhang, J.-K. E. Schemm, W. R. Higgins, and A. Kumar (2009), Evaluation of MJO forecast skill from several statistical and dynamical forecast models, *J. Clim.*, *22*, 2372–2388.
- Skamarock, W. C., et al. (2008), A description of the advanced research WRF version 3, *NCAR Tech. Note NCAR/TN-4751STR*, 113 pp, Boulder Co. [Available at [http://www.mmm.ucar.edu/wrf/users/docs/arw\\_v3\\_bw.pdf](http://www.mmm.ucar.edu/wrf/users/docs/arw_v3_bw.pdf).]
- Thompson, G., P. R. Field, R. M. Rasmussen, and W. D. Hall (2008), Explicit forecasts of winter precipitation using an improved bulk microphysics scheme. Part II: Implementation of a new snow parameterization, *Mon. Weather Rev.*, *136*, 5095–5115.
- Vitart, F., and F. Molteni (2010), Simulation of the Madden-Julian oscillation and its teleconnections in the ECMWF forecast system, *Q. R. Meteorol. Soc.*, *136*(649), 842–855.
- Wang, S., A. H. Sobel, F. Zhang, Y. Q. Sun, Y. Yue, and L. Zhou (2014), Regional simulation of the October and November MJO events observed during the CINDY/DYNAMO field campaign at gray zone resolution, *J. Clim.*, *28*, 2097–2119.
- Wheeler, M. C., and H. H. Hendon (2004), An all-season real-time multivariate MJO index: Development of an index for monitoring and prediction, *Mon. Weather Rev.*, *132*, 1917–1932.
- Yoneyama, K., C. Zhang, and C. N. Long (2013), Tracking pulses of the Madden-Julian oscillation. *Bull. Amer. Meteor. Soc.*, *94*, 1871–1891, doi:10.1175/BAMS-D-12-00157.1.
- Zhang, C., and H. H. Hendon (1997), Propagating and standing components of the intraseasonal oscillation in tropical convection, *J. Atmos. Sci.*, *54*, 741–752.